

Study of nuclear spin-lattice relaxation in the one-dimensional easy-plane ferromagnet CsNiF₃

Takao Goto

Department of Physics, College of Liberal Arts, Kyoto University, Kyoto 606, Japan

(Received 8 October 1982)

The nuclear spin-lattice relaxation time T_1 of ^{133}Cs in one-dimensional easy-plane ferromagnet CsNiF₃ has been measured with external fields between 1.5 and 12 kOe applied in the easy-magnetization plane at temperatures between 1.5 and 20 K. The primary purpose of this work is to find experimental evidence for solitons in this compound. First the experimental data are compared with the numerical calculations for the two-magnon and the three-magnon relaxation processes based on linear spin-wave theory. The data for relatively low temperatures and relatively high fields are found to be interpreted by the sum of the relaxation rates of both processes quantitatively as well as qualitatively. A significant contribution of the second-order exchange-scattered three-magnon process is revealed. For other field and temperature regions, however, there appear discrepancies between the experiment and the calculation, thus suggesting the appearance of the effect of solitons. Next we consider the relaxation mechanism due to collision between the nuclear spin and one-dimensional dilute soliton gases. This approach leads to a qualitative equation such that $T_1^{-1} \sim T^{-1} \exp(-\epsilon_s/k_B T)$, where ϵ_s is soliton activation energy given by $8S(2JSg\mu_B H)^{1/2}$. When ϵ_s/k_B is chosen as $10.3\sqrt{H}$ K (H in kOe), this equation explained well the relevant experimental data qualitatively. Quantitative calculation carried out by taking account of the contributions of the solitons passing on the nearest three linear chains resulted in the relaxation rate which is larger, by a factor of 5, compared with the data. The soliton energy obtained from the above best-fit relation is smaller by about 30% than the classical theoretical value estimated using the exchange parameters. In view of the validity of the soliton feature, the characteristics of soliton in CsNiF₃ were discussed.

I. INTRODUCTION

Recently, the sine-Gordon soliton in one-dimensional easy-plane ferromagnetic system CsNiF₃ has attracted considerable interests. Mikeska first argued that the spin Hamiltonian of CsNiF₃ with moderate external field applied in the easy-magnetization plane is equivalent to the sine-Gordon equation provided the out-of-plane spin components are neglected.¹ Subsequently Kjems and Steiner found evidence of thermally excited soliton gases from the central peak for the longitudinal spin fluctuation observed by neutron inelastic scattering.² This interpretation, however, has been the subject of some controversy; Loveluck *et al.* indicated the importance of a multimagnon difference process based on a nearly isotropic model.³ Reiter also discussed that the scattering from spin-wave density fluctuation provides a rather better interpretation.⁴ Quite recently, on the other hand, Steiner *et al.* supported the contention presented in Ref. 2 by observing the central peak for the transverse spin fluctuation.⁵

The purpose of the present work is to use nuclear magnetic relaxation to get information about the soliton dynamics in CsNiF₃ from a different standpoint. We have measured the spin-lattice relaxation time T_1 of ^{133}Cs in this compound in the temperature range from 1.5 to 20 K applying the external fields between 1.5 and 12 kOe in the easy plane.

There has already been the measurement of T_1 of ^{133}Cs for sufficiently high fields by Cohen *et al.*⁶ The experi-

mental results have been interpreted in terms of the three-magnon process by Huber and Ghosh.⁷ In order to clarify soliton contribution in T_1 of ^{133}Cs , it is first necessary to understand magnon contribution. In view of this, we compare our experimental results with the numerical calculations for the two-magnon and the three-magnon relaxation processes within the framework of linear spin-wave theory. As we shall show, a good agreement between the experiment and the calculation is obtained for relatively high fields and relatively low temperatures. For other regions, however, there appear discrepancies between them, thus suggesting the appearance of the effect of the soliton. We next consider the nuclear relaxation mechanism due to collision between the nuclear spin and one-dimensional dilute soliton gases. This approach gives a reasonable explanation of the relevant experimental data. A preliminary account of this work has already been presented in a previous paper.⁸

The crystal structure and the magnetic properties of CsNiF₃ are reviewed briefly in Sec. II. The experimental results are presented in Sec. III. Section IV is devoted to the analyses, which are followed by discussions in Sec. V.

II. CRYSTAL STRUCTURE AND MAGNETIC PROPERTIES

The crystal structure of CsNiF₃ belongs to hexagonal symmetry ($P6_3/mmc$) with the lattice constants of $a_0 = b_0 = 6.23$ Å and $c_0 = 5.21$ Å, as illustrated in Fig. 1.⁹

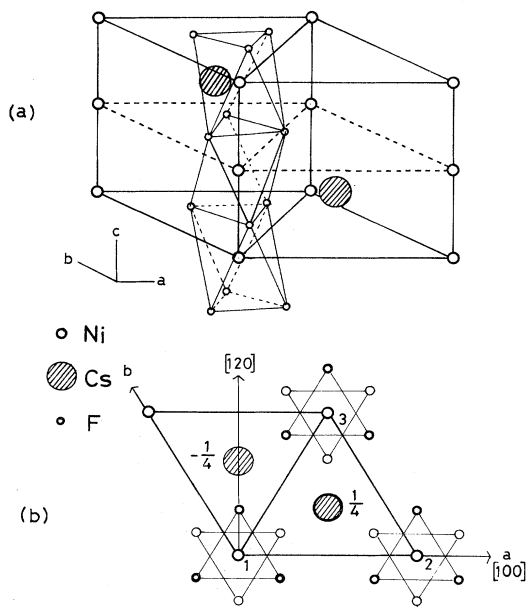


FIG. 1. Crystal structure of CsNiF₃. (a) Schematic view of the chemical unit cell. Only one of the chains along the *c* axis is shown for clarity. (b) Projection of the unit cell on the *a-b* plane.

The Ni²⁺ ions ($S=1$) compose magnetic linear chains along the *c* axis through the covalent couplings with F⁻ ions which are in trigonally distorted octahedral sites about each Ni²⁺ ion. The exchange interaction along the chain is ferromagnetic with $J/k_B=11.5$ K.^{10,11} The interchain interactions, which are antiferromagnetic, are of the order of $J'/J \approx 10^{-2}$.¹² The trigonal distortion of cubic crystalline field at the Ni²⁺ ion causes positive single-ion-type anisotropy along the *c* axis with $D/k_B=9.0$ K,^{10,11} the *a-b* plane thus being magnetic easy plane at low temperatures. A second-order phase transition to an antiferromagnetic state takes place at $T_N \approx 2.7$ K (Refs. 12–14) due to weak interchain interactions resulting mainly from the dipolar forces. Details of magnetic properties are referred to by Steiner *et al.*¹⁵

III. EXPERIMENTAL RESULTS

The experiments were performed using a coherent frequency-variable pulsed NMR spectrometer composed of Matec Inc. Models 5100 Gating Modulator, 525 rf gated amplifier, 615 tuned receiver with 253 high-impedance preamplifier, and homemade timing circuits for the pulse sequence. Conventional cryogenic technique was used in the measurements at liquid-He and liquid-H₂ temperatures. The intermediate temperatures were regulated by a standard temperature-control method using a Au + 0.07% Fe–Chromel thermocouple. A digital signal-averager system of Kawasaki Electronica, models M-50E and TMC-500, was utilized for deterioration of the signal intensity at high temperatures or at low fields.

The relaxation time T_1 was determined by observing the exponential recovery of the spin-echo signal which

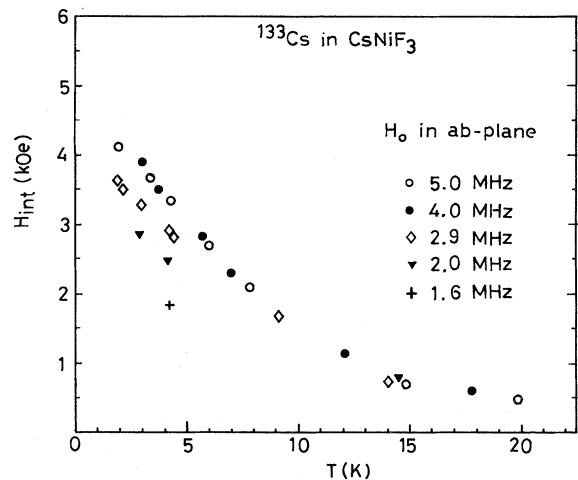


FIG. 2. Temperature dependence of field-induced internal field at the cesium nucleus obtained from the shift of the resonance field from normal value.

lasted at least over half of one decade after the saturation by a comb of rf pulses. The single crystal of CsNiF₃ was offered by Y. Yamaguchi at Electrotechnical Laboratory. The dimensions of the nearly plate-shaped crystal were of

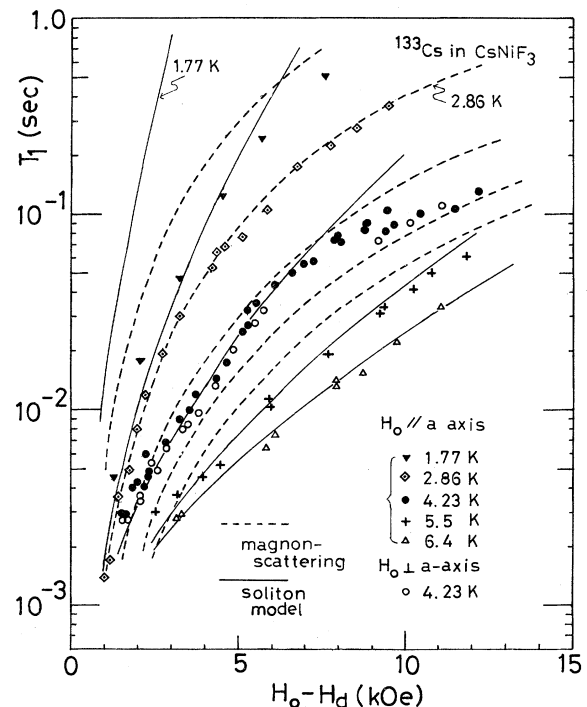


FIG. 3. Field dependence of T_1 of ¹³³Cs with the external field (H_0) applied in the *a-b* plane. The data are plotted as a function of the effective field $H'_0 = H_0 - H_d$, H_d being the demagnetizing field. The dashed lines represent the theoretical curves for $(T_1^{-1})_m = (T_1^{-1})_{2\text{ mag}} + (T_1^{-1})_{3\text{ mag}}$, which are normalized at the curve for $T=2.68$ K. The solid lines represent the best-fit curves of Eq. (4.15), which are obtained by choosing $\epsilon_s/k_B=10.3(H'_0)^{1/2}$ K.

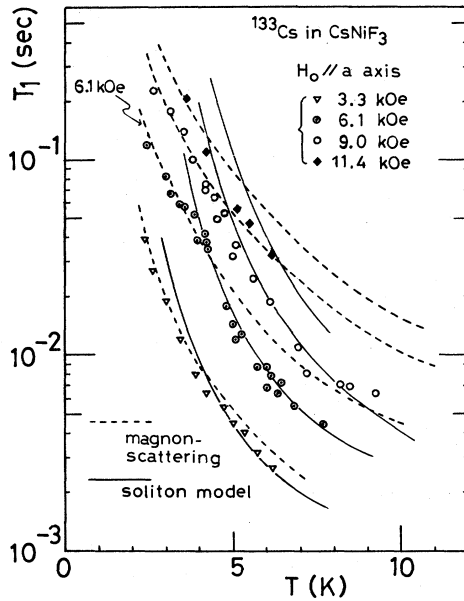


FIG. 4. Temperature dependences of T_1 of ^{133}Cs at constant fields applied along the a axis. The dashed and solid lines used have the same meanings as those in Fig. 3.

about $20 \times 4 \times 2 \text{ mm}^3$ with the c axis parallel to the longest one.

The spin-echo signal of ^{133}Cs ($I = \frac{7}{2}$) was observed as a single broad spectrum. The spectrum had a trend to broaden with increasing field and decreasing temperature. For example, the width at 4.23 K was about 300 and 800 Oe for 3 and 12 kOe, respectively. There appeared a large spin-echo amplitude modulation with a period of about $150 \mu\text{sec}$. Probably this is due to the fact that the quadrupole interaction has a small in-plane asymmetry besides a large axial asymmetry of 0.4 MHz.¹⁶ The resonance field H_0 at a constant operating frequency ω_N was always shifted from the normal values $H_{\text{res}} = \omega_N / \gamma_N + H_d - H_{\text{int}}$ ($\gamma_N = 5.585 \text{ MHz}/10 \text{ kOe}$) to the lower side. This implies that a positive internal field H_{int} is produced at the nuclear site by field-induced magnetic moments. Figure 2 shows the temperature dependences of H_{int} obtained for various operating frequencies using the relation $H_{\text{int}} = H_{\text{res}} - (H_0 - H_d)$, where H_d is the demagnetizing field. The estimation of H_d was made by calculating the demagnetization coefficients on the assumption that the shape of the specimen is an ellipsoid whose principal axes are of the same lengths as three dimensions, and by using the data of magnetization for powder.¹⁷ For instance, when H_0 is changed from 2 to 12 kOe along the longer side of the a - b plane of the specimen, the magnitude of H_d was calculated to vary from 250 to 450 Oe at 3 K and from 50 to 300 Oe at 6.4 K.

The relaxation times were measured as the function of the applied field at constant temperatures, and also as the function of the temperature at constant applied fields and at constant resonance frequencies. The experimental results are shown in Figs. 3–5. No angular dependence of T_1 was observed for H_0 in the a - b plane, as is demonstrat-

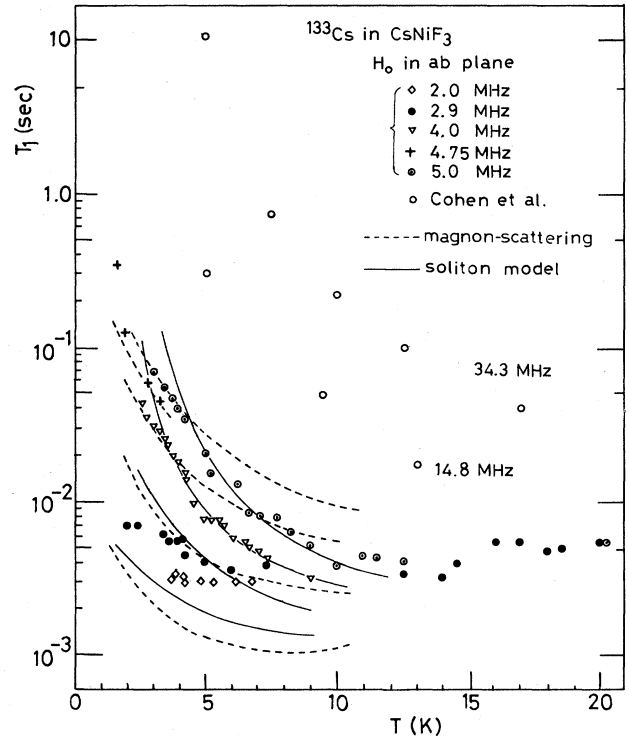


FIG. 5. Temperature dependence of T_1 of ^{133}Cs at constant resonance frequencies with $H_0 \parallel a$. The values of applied field H_0 vary depending on T according to the relation $H_0 = \omega_N / \gamma_N + H_d - H_{\text{int}}$. The dashed and the solid lines used have the same meanings as those in Fig. 3. A part of the data of Cohen *et al.* (Ref. 6) are presented for the comparison.

ed in Fig. 3 at the measurement at 4.23 K. The experimental curves exhibit remarkable field and temperature dependences. We notice that the field dependences of T_1 below and above about 4 K take somewhat different aspects, and that there appears a small bend in some of the experimental curves. These features suggest the presence of two important relaxation mechanisms. In the following section we shall examine the experimental results in view of magnon scatterings and solitons.

IV. ANALYSES

A. Nuclear Hamiltonian of ^{133}Cs

The cesium ions in CsNiF_3 are located at $(\frac{2}{3}, \frac{1}{3}, \frac{1}{4})$. We designate the Ni^{2+} spins on the j th linear chain by the suffix j and label the nearest six Ni^{2+} spin surrounding each Cs ion as $j_0 l_0$ and $j_0, l_0 + 1$ with $j_0 = 1, 2, \text{ and } 3$. (See Fig. 1.) The hyperfine and the dipolar interactions for the cesium nucleus can be described by the Hamiltonian

$$\mathcal{H}_N = \sum_{j_0=1}^3 \mathcal{H}_{\text{hyp}} + \sum_j \mathcal{H}_{\text{dip}}^{(j)} \quad (4.1)$$

with

$$\mathcal{H}_{\text{hyp}} = A \vec{I} (\vec{S}_{j_0 l_0} + \vec{S}_{j_0, l_0+1})$$

and

$$\mathcal{H}_{\text{dip}}^{(j)} = g\mu_B\gamma_N\hbar \sum_l \left[\vec{I} \cdot \vec{S}_{jl} - \frac{3(\vec{I} \cdot \vec{r}_{jl})(\vec{S}_{jl} \cdot \vec{r}_{jl})}{r_{jl}^2} \right] r_{jl}^{-3},$$

where A is the isotropic hyperfine constant and \vec{r}_{jl} is the position vector of the j th Ni^{2+} spin. The quadrupole interaction is not considered in this equation, because it is not essentially related to the present problem.

When an external field \vec{H}_0 is applied in the easy plane, the magnetic moments associated with Ni^{2+} spins are aligned along the direction of \vec{H}_0 because of the lack of in-plane anisotropy.

Let us here define the orthogonal coordinate system (x, y, z) with the z axis parallel to the applied field and the y axis along the linear chain. It proves that the transverse components of the field-induced dipole field always vanish. So the internal field H_{int} at the cesium nucleus, which is the sum of the field-induced hyperfine and the dipole fields, $H_{\text{hyp}} + H_{\text{dip}}$, is just along the z axis, and accordingly the nuclear and the electronic quantization axes coincide with each other. From Fig. 2 we find $(H_{\text{int}})_{\text{exp}} = 4.5$ kOe at 0 K. On the other hand, the magnitude of H_{dip} can be evaluated by the direct summation over a large number of lattice points. We get $H_{\text{dip}} = 0.65$ kOe for $S=1$ using $g=2.28$.¹² Thus we obtain $H_{\text{hyp}} = 3.85$ kOe, which yields hyperfine field h_f per one Ni^{2+} spin of 0.64 kOe or $A/\hbar = 2\pi \times 3.5 \times 10^5$ rad sec⁻¹.

The transverse terms of the nuclear Hamiltonian (4.1), which are responsible for the nuclear spin-lattice relaxation, are expressed as

$$\mathcal{H}'_N = \mathcal{H}'_{||} + \mathcal{H}'_{\perp} + \text{c.c.}, \quad (4.2)$$

$$\mathcal{H}'_{||} = I^+ \sum_j \sum_l D_{jl}^{(z)} S_{jl}^z, \quad (4.3)$$

$$\mathcal{H}'_{\perp} = I^+ \left[\sum_{j_0=1}^3 (A/2)(S_{j_0 l_0}^- + S_{j_0, l_0+1}^-) + (g\mu_B\gamma_N\hbar) \sum_j \sum_l (D_{jl}^{(-)} S_{jl}^- + D_{jl}^{(+)} S_{jl}^+) \right], \quad (4.4)$$

where $D_{jl}^{(z)}$ and $D_{jl}^{(\pm)}$ represent the components of the dipolar coupling tensor connecting I^+ and \vec{S}_{jl} , and c.c. designates the complex conjugate. Figure 6 shows the orthogonal coordinate system (x, y, z) in the case $\vec{H}_0 \parallel a$, which is our experimental situation, and the relationship between this system and various notations with respect to the $j_0 l_0$ th Ni^{2+} spin, which will be introduced later.

B. Relaxation process due to magnon scatterings

First we consider the nuclear spin-lattice relaxation due to magnon scatterings. The exchange Hamiltonian of the linear chain system of CsNiF_3 is expressed as

$$\mathcal{H}_{\text{ex}} = -2J \sum_l \vec{S}_l \cdot \vec{S}_{l+1} + D \sum_l (S_l^y)^2 - g\mu_B H \sum_l S_l^z \quad (4.5)$$

with $J/k_B = 11.5$ K, $D/k_B = 9.0$ K, and $g=2.28$, where H represents magnetic field in the a - b plane. Assuming that

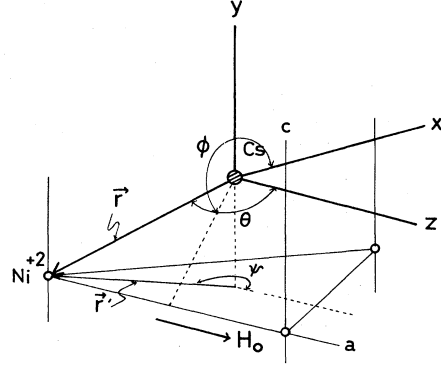


FIG. 6. Relationship between the orthogonal xyz system (z , direction of H_0 ; y , chain direction) and polar coordinates of the position vector of the $j_0 l_0$ th Ni^{2+} spin with respect to the cesium nucleus $\theta_{j_0 l_0}$ and $\phi_{j_0 l_0}$. This relation is extended to the j th Ni^{2+} spin. The vector $\vec{r}'_{j_0 l_0}$ is the projection of $r_{j_0 l_0}$ on the a - b plane, and $\psi_{j_0 l_0}$ is the angle between $\vec{r}'_{j_0 l_0}$ and the z axis. The suffixes are omitted in the figure for the clarity.

quasimagnons are well established, we apply linear spin-wave theory. Following Holstein-Primakoff representation, we introduce the Fourier-transformed magnon operators a_k^* and a_k . By transforming these operators to new normal mode operators α_k^* and α_k by a canonical transformation, $a_k = u_k \alpha_k - v_k \alpha_{-k}^*$ and $a_k^* = u_k \alpha_k^* - v_k \alpha_{-k}$, the Hamiltonian (4.5) is diagonalized as

$$\mathcal{H}_{\text{ex}} = \hbar\omega_k \alpha_k^* \alpha_k + E_0, \quad (4.6)$$

$$\hbar\omega_k = \epsilon_k = [\chi_k^2 - (D'S)^2]^{1/2},$$

with $D' = (S - \frac{1}{2})D/S$ and $\chi_k = 4JS[1 - \cos(ka)] + D'S + g\mu_B H$, where a is the lattice spacing along the chain, and D is modified by a quantum correction factor.¹⁸ The coefficients u_k and v_k are given by

$$u_k = \cosh\theta_k$$

and

$$v_k = \sinh\theta_k$$

with

$$\tanh(2\theta_k) = D'S/\chi_k.$$

The relaxation rates due to magnon scatterings can be obtained on the basis of the standard formula by expressing the electron spin operators in Eq. (4.2) with the magnon operators. The first term $\mathcal{H}'_{||}$, Eq. (4.3), induces the two-magnon (2 mag) process in which annihilation of one magnon and simultaneous creation of another magnon occurs when the nuclear spin flips. The relaxation rate for this process is given by

$$(T_1^{-1})_{2 \text{ mag}} = \frac{4\pi}{\hbar N^2} (g\mu_B\gamma_N\hbar)^2 G \times \sum_{k, k'} (u_k u_{k'} + v_k v_{k'})^2 \langle n_k \rangle (\langle n_{k'} \rangle + 1) \times \delta(\epsilon_k - \epsilon_{k'} - \hbar\omega_N), \quad (4.7)$$

where N is the total number of the electron spins on a

TABLE I. Numerical values of geometrical factors and coupling constants for the two-magnon and the three-magnon processes.

Geometrical factor	Autocorrelation		Pair correlation	
	$l'=l$	$l'=l+1$	$l'=l+1$	$l'=l+2$
G (10^{45} cm ⁻⁶)	3.12	1.49	0.013	
G' (10^{45} cm ⁻⁶)	2.87	1.04	0.034	
G'' (10^{22} cm ⁻³)	-1.73	-0.561	0	
Coupling constant (10^{-41} erg ²)				
Two-magnon process	$(g\mu_B\gamma_N\hbar)^2G$		2.83	
Three-magnon process	$12\left[\frac{A}{2}\right]^2$		1.53	4.12
	$(gu_B\gamma_N\hbar)^2G'$		2.39	
	$(g\mu_B\gamma_N\hbar)G''\left[\frac{A}{2}\right]$		0.202	

linear chain, $\hbar\omega_N$ is the nuclear Zeeman energy, and $\langle n_k \rangle$ is the Bose-Einstein distribution function for the number of magnons. In this equation, G is the geometrical factor, and is expressed as

$$G = \sum_j \sum_{l,l'} \frac{9}{4} r_{jl}^{-3} r_{jl'}^{-3} \sin(2\theta_{jl}) \sin(2\theta_{jl'}) \cos(\phi_{jl} - \phi_{jl'}), \quad (4.8)$$

where θ_{jl} and ϕ_{jl} are polar angles of r_{jl} . (See Fig. 6.)

We here assumed that the time pair correlations of different electron spins on each linear chain are equal to the time autocorrelations of the individual electron spins. Hence the effect of the interference of the different spins appears only in the geometrical factor. The value of the geometrical factor for the pair correlation diminishes very rapidly as the distance of the relevant two spins increases. (See Table I.) Thus the above assumption applies only to the nearest, and at most the second-nearest two spins.

Another term \mathcal{H}'_1 , Eq. (4.4) brings about the three-

magnon process, as the lowest-order process, in which the nuclear spin flip is accompanied by annihilation (creation) of one magnon and simultaneous creation (annihilation) of two magnons. This process requires, on the basis of energy conservation, that twice the minimum magnon energy must not exceed the maximum energy. As is seen from the dispersion relation (4.6) this condition is satisfied as long as the applied field is not extremely strong. This is the present case.

Now let us consider the second-order exchange-scattered three-magnon process.¹⁹ This process takes place through the perturbation interactions like I^+S^- in Eq. (4.4) in such a way that a virtual magnon emitted by the nuclear spin flip and thermal magnons interact with each other via the four-magnon terms of the exchange interaction, thus resulting in scattering of three thermal magnons.

Similarly terms like I^+S^+ in Eq. (4.4) cause the second-order process which accompanies the absorption of a virtual magnon. The four-magnon exchange-scattering terms of the exchange Hamiltonian (4.5) are expressed in terms of the magnon operators a_k^* and a_k as follows:

$$\mathcal{H}'_{\text{ex}} = \frac{2J}{N} \sum_{k_1, k_2, k_3, k_4} \gamma(k_1, k_2, k_3, k_4) a_{k_1}^* a_{k_2}^* a_{k_3} a_{k_4} \times \delta(k_1 + k_2 - k_3 - k_4) \quad (4.9)$$

with

$$\begin{aligned} \gamma(k_1, k_2, k_3, k_4) = & \cos[(k_2 - k_4)a] \\ & - \frac{1}{4} [\cos(k_1 a) + \cos(k_2 a) \\ & + \cos(k_3 a) + \cos(k_4 a)] + \frac{D}{4J}. \end{aligned}$$

By combining this with the one-magnon term $\mathcal{H}'_1^{(1)}$ of Eq. (4.4), the effective perturbation interaction is given as

$$\mathcal{H}'_{\text{eff}} = 2\mathcal{H}'_{\text{ex}}(\mathcal{H}'_1^{(1)}/\epsilon'_k), \quad (4.10)$$

where ϵ'_k represent the virtual-magnon energy, and the prefactor 2 results from the participation of two virtual magnons with wave vectors k_3 and k_4 or k_1 and k_2 . The total perturbation interaction for the three-magnon (3 mag) process is then given by the sum of the first-order interaction and the above second-order interaction. We obtain the following expression for the relaxation rate:

$$\begin{aligned} (T_1^{-1})_{3 \text{ mag}} = & \frac{\pi}{\hbar S N^3} C \sum_{1,2,3} \left[1 + \frac{16JS}{\epsilon_4} \gamma(1,2,3,4) \right]^2 \left[u_1^2 u_2^2 u_3^2 + v_1^2 v_2^2 v_3^2 + 2v_1^2 u_2^2 v_3^2 + 2u_1^2 v_2^2 u_3^2 \right. \\ & \left. + 2u_1 u_2 u_3 v_1 v_2 v_3 \left(\frac{u_1}{v_1} + \frac{u_2}{v_2} + \frac{u_3}{v_3} + \frac{v_1}{u_1} + \frac{v_2}{u_2} + \frac{v_3}{u_3} \right) \right] \\ & \times \langle n_1 \rangle \langle n_2 \rangle (\langle n_3 \rangle + 1) \delta(\epsilon_1 + \epsilon_2 - \epsilon_3 - \hbar\omega_N) \end{aligned} \quad (4.11)$$

with $k_4 = k_1 + k_2 - k_3$, where 1, 2, 3, and 4 refer, respectively, to the wave vectors k_1 , k_2 , k_3 , and k_4 , and C

represents the coupling constant. In this equation, the first and the second terms in the first set of large

parentheses represent the direct three-magnon contribution and the exchange-scattering contribution, respectively. The coupling constant C is given by

$$C = 12 \left[\frac{A}{2} \right]^2 + (g\mu_B\gamma_N\hbar)^2 G' + (g\mu_B\gamma_N\hbar) G'' \left[\frac{A}{2} \right] \quad (4.12)$$

with

$$G' = \sum_j \sum_{l,l'} [1 - \frac{3}{2}(\sin^2\theta_{jl} + \sin^2\theta_{j'l'}) + \frac{9}{2}\sin^2\theta_{jl}\sin^2\theta_{j'l'}\cos^2(\phi_{jl} - \phi_{j'l'})] r_{jl}^{-3} r_{j'l'}^{-3}$$

and

$$G'' = \sum_{j_0=1}^3 \sum_{l,l'=l_0}^{l_0+1} [(1 - \frac{3}{2}\sin^2\theta_{j_0 l}) r_{j_0 l}^{-3} + (1 - \frac{3}{2}\sin^2\theta_{j_0 l'}) r_{j_0 l'}^{-3}],$$

where the meanings of the various notations are described in Sec. IV A and Eq. (4.1). The first and the second terms are due to the hyperfine and the dipolar interactions alone,

respectively, and the third term corresponds to the interference between them. In deriving the above equation, we have assumed that the time pair correlations of the two different spins are equal to the time auto correlations of the individual spins as in the case of the two-magnon process.

We here define the state density of magnons from dispersion relation (4.6). It is given by

$$N(\epsilon_k) = \epsilon_k [4JSa \sin(ka)\chi_k]^{-1}. \quad (4.13)$$

With the use of $N(\epsilon_k)$, the sums with respect to the wave vectors in Eqs. (4.7) and (4.11) are replaced, respectively, by the integral and the double integral with respect to the magnon energy. Then, as is seen from the above expression, $N(\epsilon_k)$ has a singularity associated with one dimensionality at $k=0$ or at the magnon gap energy. To avoid the resulting divergence of the integral, we cut off, following Huber and Ghosh,⁷ the lower limit of the integral at $k=\xi^{-1}$, where ξ is the correlation length of the one-dimensional planar system which is given as $\xi=8J/k_B T$. The integrals were then performed numerically on a computer. The geometrical factors were also calculated by direct summation over the lattice points of $10 \times 10 \times 20$

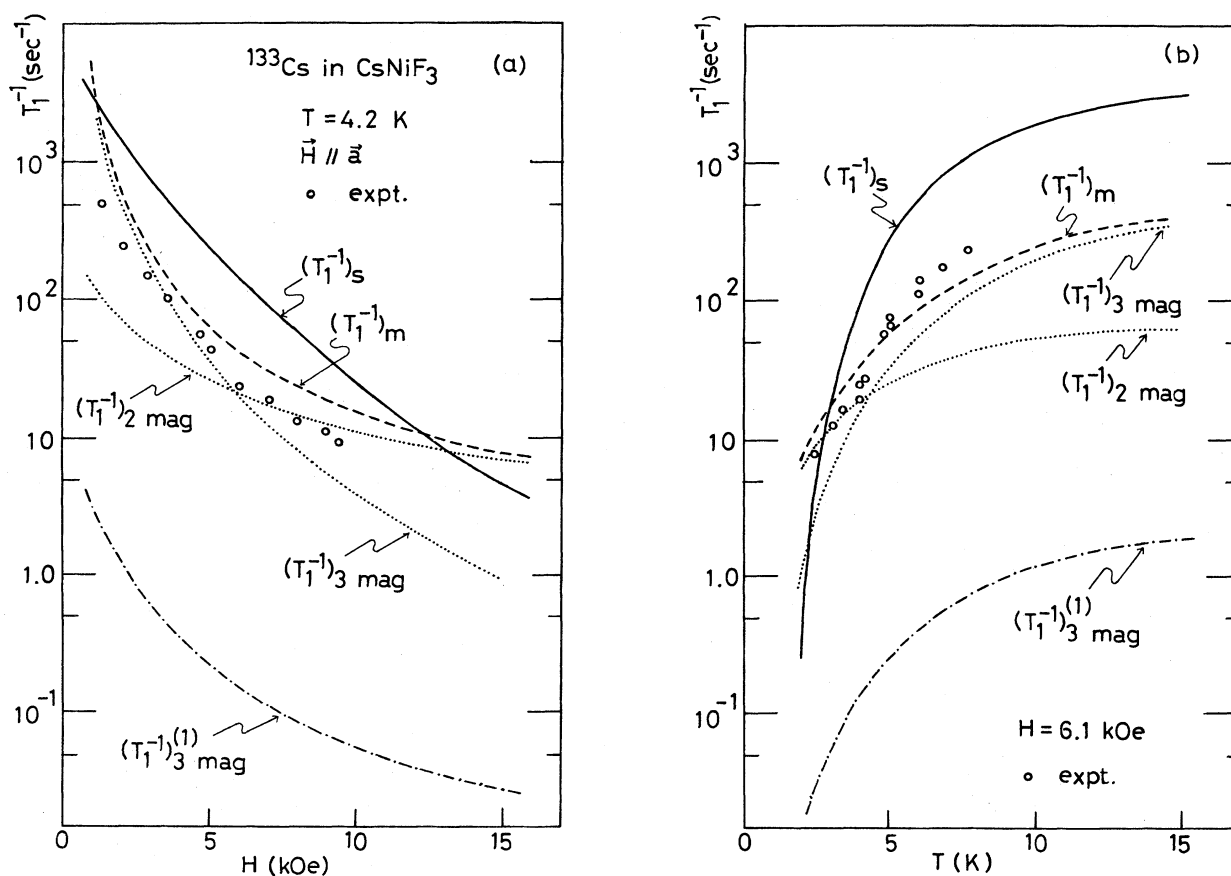


FIG. 7. Results of the numerical calculations for the relaxation rates for magnon-scattering processes and for soliton model: \cdots , $(T_1^{-1})_{2 \text{ mag}}$, $(T_1^{-1})_{3 \text{ mag}}$ (exchange-enhanced process); $---$, $(T_1^{-1})_m = (T_1^{-1})_{2 \text{ mag}} + (T_1^{-1})_{3 \text{ mag}}$; $- \cdot - \cdot$, $(T_1^{-1})_{3 \text{ mag}}^{(1)}$ (the first-order three-magnon process); and $---$, $(T_1^{-1})_s$ (soliton model). (a) Field dependences at $T=4.2$ K. (b) Temperature dependences at $H_0=6.1$ kOe. A part of the data are shown.

along the crystal axes. The numerical values of these factors and the coupling constants for the two processes are given in Table I. In these calculations, we used the numerical values of $J/k_B=11.5$ K, $D/k_B=9.0$ K, $g=2.28$, and $A/\hbar=2\pi\times 3.5\times 10^5$ rad sec⁻¹.

Typical examples of the calculated field and temperature dependences of $(T_1^{-1})_{2\text{ mag}}$ and $(T_1^{-1})_{3\text{ mag}}$ are shown by the dotted lines in Fig. 7 together with the corresponding experimental values. As is seen, the magnitudes of both rates are of comparable order to each other. Thus the relaxation rate is determined by the sum of the rates for both processes, which is given by the dashed line in the figure. The dot-dashed line in Fig. 7 represents the relaxation rate for the first-order three-magnon process calculated similarly.²⁰

As is seen, the contribution of the second-order exchange enhanced process is very significant. The enhancement factor is about 2 orders of magnitude. In Figs. 3–5, we represent by the dashed line the calculated curves for T_1 corresponding to the experimental curves, which are normalized at the curves for $T=2.68$ K, $H_0=6.1$ kOe, and $\omega_N=5.0$ MHz, respectively. The qualitative agreement between the experiment and the calculation is good for the relatively low temperatures and the relatively high fields. As is also seen in Fig. 7, the calculated values for the relaxation rate agree with the experimental values within the difference of a factor. Thus the quantitative agreement between the experiment and the calculation is satisfactory as well. Although both the two-magnon and the three-magnon processes are effective in the present field and temperature regions, it is difficult to identify the two relaxation mechanisms distinguished in our experimental curves as these two processes alone. Note that the total relaxation rate exhibits a rather smooth curve, and

that the two-magnon process predicts by itself much more gentle behavior of T_1 than the experimental features. We suppose the deviation of the experimental curves from the theoretical prediction of the magnon-scattering process is due to soliton contribution.

C. Soliton model

We will now proceed to the soliton model. Let us suppose a soliton passing on the linear chain of CsNiF₃. The resulting 2π rotation of the electron spins in the easy plane gives rise to the time-dependent transverse interaction with collisions of nonmagnetic ideal gases. The dynamics of a nuclear spin based on such a model has been studied theoretically by Huber.²¹ He obtained the transition probability of the nuclear spin flip by applying the theory for nonadiabatic level crossing in atomic collision. His theory, however, does not include explicitly the effect of the applied field which plays an essential role in the soliton in CsNiF₃. It also turns out that the level crossing is not guaranteed in our case because of the actual Zeeman splitting which is much larger than the magnitudes of the hyperfine and the dipolar interactions.

We here evaluate the transition probability using the analogy of our problem to the nuclear magnetic relaxation in nonmagnetic monoatomic gases.²² Then we derive the equation for the relaxation rate following the procedure presented in Huber's paper.²¹ The essentials are referred to in our previous paper.⁸

The following is our final result:

$$(T_1^{-1})_s = \frac{32}{\sqrt{3\pi}} \left[\frac{4AS}{\hbar} \right]^2 S \left[\frac{2J}{D} \right]^{1/2} \frac{\hbar}{k_B T} \exp \left[-\frac{\epsilon_s}{k_B T} \right] \left\{ \frac{3}{2} - \gamma + \ln \left[\frac{1}{2} \left[\frac{\hbar}{4AS} \right] \left[\frac{3Dk_B T g \mu_B H}{2JS\hbar^2} \right]^{1/2} \right] \right\} \quad (4.14)$$

with $\epsilon_s = 8S(2JSg\mu_B H)^{1/2}$, where ϵ_s is soliton (antisoliton) activation energy, and γ is Euler's constant.

Here only the hyperfine interactions with the two nearest Ni²⁺ spins on the linear chain were considered temporarily. As is shown later, the term in the curly bracket in the above equation is almost constant in our experimental condition. The relaxation rate is thus described qualitatively as

$$(T_1^{-1})_s \sim T^{-1} \exp(-c\sqrt{H}/T) \quad (4.15)$$

with $c = 8S(2JSg\mu_B)^{1/2}/k_B$.

The best fitting of Eq. (4.15) to the experimental results was obtained by choosing $c_{\text{expt}} = 10.3$ K (kOe)^{-1/2}. The results are shown in Figs. 3–5 by the solid line. The value of c_{expt} is smaller by about 30% than the theoretical value c_{theor} calculated using the exchange parameters. The use of c_{theor} in Eq. (4.15) resulted in much more rapid field

and temperature dependences of T_1 as compared with the experimental curves. As is seen in these figures, the experimental data which deviate from the prediction of the magnon-scattering relaxation process are reasonably explained by the above equation.

Next, to make a quantitative comparison between the theory and the experiment, we shall evaluate the coupling constant for Eq. (4.14) properly. The predominant contributions result from the nearest six Ni²⁺ spins on the three linear chains via the hyperfine and the dipolar interactions. We consider only these three linear chains. When one soliton passes on one of these chains, which is labeled as j_s , the time-dependent transverse field $H_N^x(t)$ along the x direction is caused by the rotating spins on the j_s chain and the stationary spins on the other chains. The latter contribution emerges as a result of the breakdown of the cancellation of the transverse components of the static dipole field.

The phase angle of the rotating spin is given, in the con-

tinuum and nonrelativistic limits, as

$$\phi(t) = 4 \tan^{-1} \exp \left[-\frac{y-vt}{da} \right], \quad (4.16)$$

$$H_N^x(t) = \sum_{j_0 \neq j_s} \sum_l \frac{3g\mu_B S r_{j_0 l}'^2}{2r_{j_0 l}^5} \sin(2\psi_{j_0 l}) + \left[2AS/\gamma_N \hbar + \sum_l \frac{g\mu_B S}{r_{j_0 l}^3} \left[\frac{3r_{j_0 l}'^2}{r_{j_0 l}^2} \cos^2 \psi_{j_s l}(t) - 1 \right] \right] \sin \phi(t) + \sum_l \frac{3g\mu_B S r_{j_s l}'^2}{2r_{j_s l}^5} \sin[2\psi_{j_s l}(t)] \cos \phi(t) \quad (4.17)$$

with $\psi_{j_s l}(t) = (\psi_{j_s l})_{\phi(t)=0} - \phi(t)$, where $r_{j_0 l}'$ is the projection of $r_{j_0 l}$ to the a - b plane, and $\psi_{j_0 l}$ is the angle between the z axis and $r_{j_0 l}'$. (See Fig. 6.) In the above expression, we have neglected the phase lags of the rotating electron spins, considering the fact that only the nearest and at most, the second-nearest spins are effective actually.

The perturbation interaction is given by

$$\mathcal{H}'_N(t) = -\gamma_N \hbar H_N^x(t) I^x.$$

The time dependences of $\sin[\phi(t)]$ and $\cos[\phi(t)-1]$ are shown in Fig. 8. As is seen, the first and the second terms of $H_N^x(t)$ are effective only for the durations $0 < |t| \lesssim 4\tau_0$ and $0 < |t| \lesssim 2\tau_0$ with $\tau_0 = da/v$, respectively.

Keeping this in mind, we here use the simple approximations such that

$$\sin \phi(t) \rightarrow (8\tau_0)^{-1} \int_{-\infty}^{+\infty} |\sin \phi(t)| dt = \begin{cases} \frac{1}{2}, & -4\tau_0 \leq t < 0 \\ -\frac{1}{2}, & 0 < t \leq 4\tau_0 \end{cases} \quad (4.18)$$

and

$$\cos \phi(t) - 1 \rightarrow (4\tau_0)^{-1} \int_{-\infty}^{+\infty} [\cos \phi(t) - 1] dt = -1, \quad 0 < |t| \leq 2\tau_0, \quad (4.19)$$

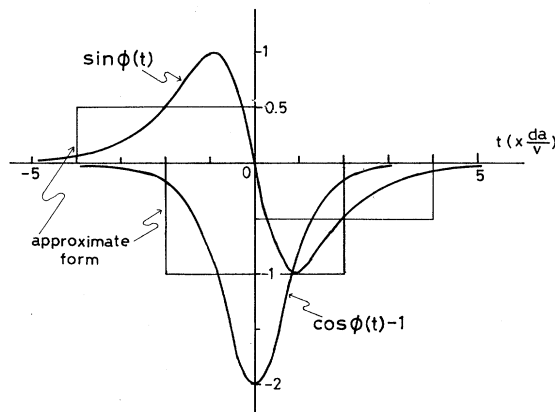


FIG. 8. Behaviors of $\sin \phi(t)$ and $\cos \phi(t) - 1$ associated with the passing of one soliton. The soliton is assumed to be centered at $t=0$. Narrow lines represent the approximate square-wave forms used in the evaluation of the probability amplitude for the nuclear relaxation.

where v is the soliton velocity and d is the characteristic scale of soliton width in units of the lattice spacing a . Then, referring to Eq. (4.1), we obtain the following expression for $H_N^x(t)$:

and 0 otherwise. (See Fig. 8.) Then, we approximate $H_N^x(t)$ as the following stepwise function:

$$H_N^x(t) = \begin{cases} P_1, & -4\tau_0 \leq t < -2\tau_0 \\ P_1 - P_2, & -2\tau_0 \leq t < 0 \\ -P_1 - P_2, & 0 < t \leq 2\tau_0 \\ -P_1, & 2\tau_0 < t \leq 4\tau_0 \end{cases} \quad (4.20)$$

with

$$P_1 = h_f + \frac{3}{2} B_1 \sin^2 \psi_{j_s} - \frac{B_2}{2}$$

and

$$P_2 = \frac{B_1}{2} \sin(2\psi_{j_s}),$$

where

$$B_1 = \sum_l g\mu_B S r_{j_0 l}'^2 / r_{j_0 l}^5, \quad B_2 = \sum_l g\mu_B S / r_{j_0 l}^3,$$

and $h_f = AS/\gamma_N \hbar$.

The probability amplitude for the nuclear transition during each of the above time intervals $2\tau_0$ is taken to be of the order of $q \simeq \gamma_N H_N^x(2\tau_0)$, where H_N^x stands for the respective amplitudes of $H_N^x(t)$. The transition probability w for the perturbation interaction (4.20) is then given by

$$w = [2P_1^2 + (P_1 - P_2)^2 + (P_1 + P_2)^2] \gamma_N^2 (2\tau_0)^2. \quad (4.21)$$

We here rewrite this as

$$w = 2q'^2 \simeq 4(1 - \cos q') \quad (4.22)$$

with $q' = 2(2P_1^2 + P_2^2)^{1/2} \gamma_N \tau_0$.

We are concerned with the case $q' \ll 1$. This will be discussed later. If we consider only the hyperfine interaction in the perturbation interaction (4.20), we get the transition probability $w_0 = 2q^2$ with $q = (AS/\hbar)4\tau_0$. Equation (4.14) has been obtained using w_0 . Comparing w and w_0 , we find the coupling constant which replaces $(4AS/\hbar)$ in Eq. (4.14) to be

$$C(j_s) = 2(2P_1^2 + P_2^2)^{1/2} \gamma_N. \quad (4.23)$$

It is noted that $C(j_s)$ varies depending on whether $j_s = 1, 2, \text{ or } 3$, that is, which of the three chains the soliton passes

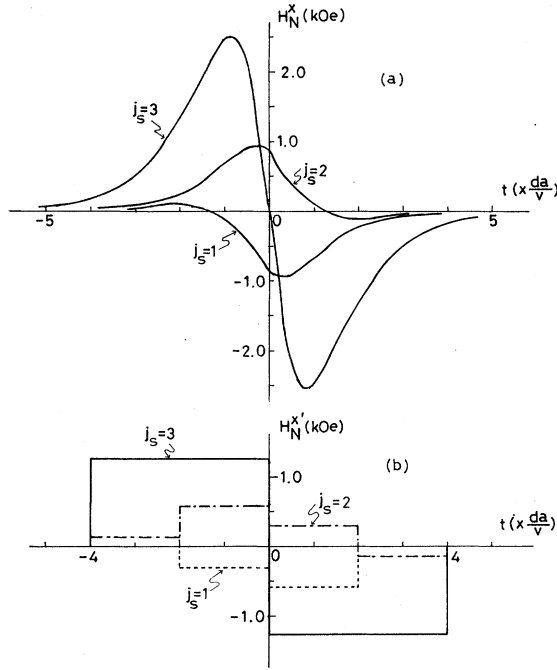


FIG. 9. (a) Time dependences of the perturbation field $H_N^x(t)$ at the cesium nucleus, which are caused by a soliton passing on one of the three nearest chains denoted in Fig. 1(b) as 1, 2, and 3. (b) Corresponding approximate stepwise forms used in the calculation of the coupling constant in Eq. (4.24).

on. Using the best-fit value c_{expt} for the soliton energy, we obtain the following equation:

$$(T_1^{-1})_s = \frac{32\hbar s}{\sqrt{3\pi}} \left[\frac{2J}{D} \right]^{1/2} \left[\sum_{j_s=1}^3 C(j_s)^2 \{C(j_s)\} \right] \times (k_B T)^{-1} \exp(-10.3\sqrt{H}/T), \quad (4.24)$$

where H is in units of kOe, and $\{C(j_s)\}$ means the term of the curly bracket in Eq. (4.14).

In the case $H_0 \parallel [100]$, we have $C(j_s=1)=C(j_s=2)$. Taking the lattice sums up to the third-nearest points on the linear chain, we get $B_1=820$ Oe and $B_2=1140$ Oe. We have also obtained $h_f=640$ Oe in Sec. IV A. Using these values, we obtain $C(j_s=1,2)=1.2 \times 10^3 \gamma_N$ and $C(j_s=3)=3.6 \times 10^3 \gamma_N$ in units of sec^{-1} . Figure 9 shows the time dependences of $H_N^x(t)$ and the corresponding approximate forms $H_N^x(t)$ for $j_s=1, 2$, and 3. The numerical values for $(T_1^{-1})_s$ were then calculated from Eq. (4.24). A part of the results are shown in Fig. 8 by the solid line. As is seen, the calculated relaxation rate is larger than the experimental values by a factor of 5 over the whole relevant regions. Such a quantitative disagreement seems not to be so serious considering the classical model for the soliton in CsNiF₃ and some approximations which were used in deriving the equation for the relaxation rate.

V. DISCUSSION

As is seen in Figs. 3–5, the field and the temperature regions where the soliton model is valid extend over ap-

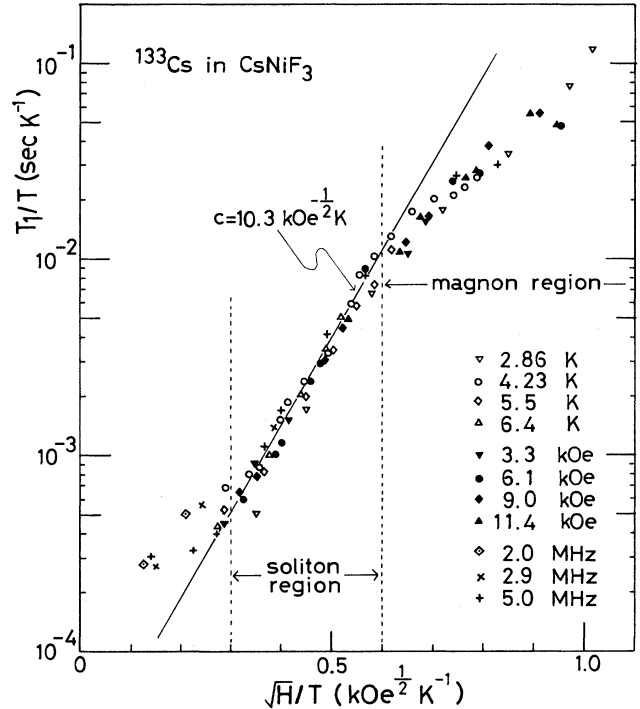


FIG. 10. Plot of $\ln(T_1/T)$ vs \sqrt{H}/T with $H=H_0-H_d$ for the experimental results based on Eq. (4.15). Solid line represents the best-fit curve of Eq. (4.15) obtained by choosing $c=10.3 \text{ kOe}^{-1/2} \text{K}$.

proximately from 2 to 11 kOe and from 3 to 10 K. These regions have a trend to shift to higher sides with increasing temperature and increasing field, respectively. Let us here plot the experimental data with \sqrt{H}/T ($H=H_0-H_d$ in units of kOe) as abscissa against $\ln(T_1/T)$ as ordinate according to Eq. (4.15). The result is shown in Fig. 10. As is demonstrated, all of the plotted points for $0.3 \lesssim \sqrt{H}/T \lesssim 0.6$ lie in parallel with the solid line, which represents the prediction of Eq. (4.15) with the best-fit value of c_{expt} . On the other hand, the points for $\sqrt{H}/T \gtrsim 0.6$, which have been interpreted by the magnon scattering, deviate from the solid line definitely. The points for low fields and high temperatures such that $\sqrt{H}/T \lesssim 0.3$ scatter appreciably. Thus we may infer that the soliton picture is adequate in CsNiF₃ for the field and the temperature regions which satisfy $0.3 \lesssim \sqrt{H}/T \lesssim 0.6$ in units of $\text{kOe}^{1/2} \text{K}^{-1}$. It should be added that the quantitative agreement between the experiment and the calculation has been satisfactory as well.

It is interesting to examine the characteristics of the soliton in CsNiF₃. Table II gives a summary of the numerical calculations of various physical quantities for typical values of H and for the boundary values of \sqrt{H}/T . The theoretical (classical) and the experimental values have been obtained using the exchange parameters and the best-fit relations for the soliton energy $(\epsilon_s/k_B)_{\text{expt}}=10.3 \sqrt{H} \text{K}$, respectively. It should be noted that the difference of about 30% in the soliton energy between these values is consistent with the result for the neutron inelastic scatter-

TABLE II. Numerical representation of the characteristics of soliton in CsNiF₃. The numerical values were calculated using the exchange parameters according to the classical expressions as given below. The values with an asterisk were obtained using our best-fit relation $\epsilon_s/k_B = 10.3\sqrt{HK}$, H being in units of kOe. The unit a is the lattice spacing along the chain; $a = c_0/2 = 2.605 \times 10^{-8}$ cm.

H (kOe)	d^a (\AA)	M_s^b (g)	ϵ_s/k_B^c (K)	\sqrt{HT}^{-1} (kOe ^{1/2} /K)	$\langle v_s \rangle^d$ (a/sec) (cm/sec)	n_s^e (a^{-1}) (cm ⁻¹)	n_s^{-1} (a) (cm)	t_c^f (sec)
2.0	8.7	6.0×10^{-25}	21.2 (14.6*)	0.3	3.3×10^{11}	$1.0 \times 10^{-2*}$	$1.0 \times 10^{2*}$	$3.0 \times 10^{-10*}$
10	3.9	1.3×10^{-24}	47.5 (32.6*)	0.6	8.7×10^3	$3.8 \times 10^{5*}$	$2.6 \times 10^{-6*}$	
					2.4×10^{11}	$7.1 \times 10^{-4*}$	$1.4 \times 10^{3*}$	$5.9 \times 10^{-9*}$
					6.2×10^3	2.7×10^4	$3.0 \times 10^{-5*}$	

$$^a d (\text{width}) = (2JS/g\mu_B H)^{1/2}.$$

$$^b M_s (\text{mass}) = 4\hbar^2/a^2 Dd.$$

$$^c \epsilon_s (\text{energy}) = 8S(2JSg\mu_B H)^{1/2}.$$

$$^d \langle v_s \rangle (\text{mean velocity}) = (2k_B T/\pi M_s)^{1/2}.$$

$$^e n_s (\text{density}) = (da)^{-1}(2\epsilon_s/\pi k_B T)^{1/2} \exp(-\epsilon_s/k_B T).$$

$$^f t_c (\text{mean collision time}) = n_s^{-1}/\langle v_s \rangle.$$

ing. Quite recently Mikeska²³ has indicated that the soliton energy for the spin system of CsNiF₃ becomes about 10% below the classical value due to the quantum correction.

Thus our value of the soliton energy may be said to be reasonable. Looking at the numerical values in Table II, we find that the characteristics of the soliton in CsNiF₃ resemble those of actual ideal gases. For the N₂ molecules (radius $r_0 = 1.9$ Å) at 0°C and 760 Torr, for example, we have the following values: m (mass) = 4.6×10^{-24} g, n_{N_2} (density) = 2.7×10^{19} cm⁻³, $\langle v_{N_2} \rangle$ (mean thermal velocity) = $(3k_B T/m)^{1/2} = 4.5 \times 10^{45}$ cm/sec, $(t_c)_{N_2}$ (mean collision time) = $(\pi m/k_B T)/(4n_{N_2} 4\pi r_0^2) = 1.3 \times 10^{-10}$ sec, l (mean free path) = $(t_c)_{N_2} \langle v_{N_2} \rangle = 5.8 \times 10^{-6}$ cm. (As for the density, the difference in the dimensionality must be considered.)

The average duration of the collisions between the nuclear spin and the soliton gases, which is given by $\tau_c = da/\langle v_s \rangle$, is found to be of the order of 10^{-11} sec. For example, this value yields the probability amplitude of $q' \simeq 10^{-4}$ for the coupling constant $C(j_s = 3) = 3.6 \times 10^3 \gamma_N$. [Refer to Eqs. (4.20) and (4.23).] Thus the use of the approximation $q'^2 \simeq 2(1 - \cos q')$ in Eq. (4.22) may be justified for almost all soliton gases whose velocities are determined by the one-dimensional distribution function. We also find that the average duration of the collisions is much less than the nuclear Lamour period ω_N^{-1} .

The term in the curly bracket in Eq. (4.24) is given as $\ln[5.7 \times 10^{10} HT/2C(j_s)]$. When we apply $C(j_s = 3) = 3.6 \times 10^3 \gamma_N$, this term takes, for example, the values of 9.1 for $H = 2$ kOe and $T = 4$ K and 10.4 for $H = 10$ kOe and 10 K. Only slight field and temperature dependences arise from this term over the whole regions where the soliton model is applied. We, therefore, used Eq. (4.15) in the procedure of the qualitative fitting between the experiment and the theory.

Borsa²⁴ has discussed independently the nuclear spin-lattice relaxation due to sine-Gordon soliton on the basis of the same theoretical background as ours. He obtained the following equation for a ferromagnetic chain:

$$T_1^{-1} \sim HT^{-1} \exp(-c\sqrt{H}/T).$$

This equation differs from our result, Eq. (4.15), in its field dependence. In deriving this equation, the average duration of the collisions between the nuclear spin and the soliton gases has been taken as $\tau_f = b/\langle v_s \rangle$, where b is a field-independent distance of closest approach. We think the parameter b should be identified as the soliton width which has the field dependence like $H^{-1/2}$. In this case, Borsa's result agrees with our result essentially.

To summarize, we have investigated T_1 of ¹³³Cs in CsNiF₃ for the purpose of finding experimental evidence for solitons. The experimental results were first compared with the numerical calculations for the two-magnon and the three-magnon relaxation processes carried out within the framework of linear spin-wave theory.

The experimental results for relatively low temperatures and relatively high fields were found to be interpreted by the sum of the relaxation rates for both processes. There have appeared deviations of the data for other regions from the predictions of the magnon-scattering relaxation mechanism. A theoretical approach based on one-dimensional dilute soliton gas model explained such experimental situations reasonably. Although the possibility of the higher-order magnon scattering is not necessarily ruled out, it seems unlikely that such processes result in a rather simple behavior of T_1 as was observed over the wide field and temperature ranges. We believe the present work may provide experimental evidence for solitons in CsNiF₃.

ACKNOWLEDGMENTS

The author wishes to thank Dr. Y. Yamaguchi at Electrotechnical Laboratory for his offering the single crystal of CsNiF₃ and Dr. Y. Ajiro for illuminating discussions which motivated the present work. Thanks are also due to Professor T. Kawai, Professor S. Hatano, Professor T. Kawasaki, and Dr. S. Maegawa for valuable discussions. The x-ray analysis for the identification of the crystal axes by Professor H. Kiho is gratefully acknowledged.

- ¹H. J. Mikeska, *J. Phys. C* **11**, L29 (1978).
- ²J. K. Kjems and M. Steiner, *Phys. Rev. Lett.* **41**, 1137 (1978).
- ³J. M. Loveluck, T. Schneider, E. Stoll, and H. R. Jauslin, *Phys. Rev. Lett.* **45**, 1505 (1980).
- ⁴G. Reiter, *Phys. Rev. Lett.* **46**, 202 (1981); **46**, 518 (1981).
- ⁵M. Steiner, K. Kakurai, W. Knop, R. Pynn, and J. K. Kjems, *Solid State Commun.* **41**, 329 (1982).
- ⁶A. Cohen, E. Ehrenfreund, and H. J. Guggenheim, *J. Magn. Magn. Mater.* **7**, 220 (1978).
- ⁷D. L. Huber and K. Ghosh, Conference on Magnetism and Magnetic Materials, New York, 1979 [*J. Appl. Phys.* **50**, 7740 (1979)].
- ⁸T. Goto and Y. Yamaguchi, *J. Phys. Soc. Jpn.* **50**, 2133 (1981).
- ⁹D. Babel, *Z. Anorg. Allg. Chem.* **369**, 117 (1969).
- ¹⁰M. Steiner, B. Doner, and J. Villain, *J. Phys. C* **8**, 165 (1975).
- ¹¹M. Steiner and J. K. Kjems, *J. Phys. C* **10**, 2665 (1977).
- ¹²J. V. Levesque, J. Snell, and J. J. Smit, *Solid State Commun.* **13**, 371 (1973).
- ¹³M. Steiner, *Z. Angew. Phys.* **32**, 116 (1971).
- ¹⁴M. Steiner, *Solid State Commun.* **11**, 73 (1972).
- ¹⁵M. Steiner, J. Villain, and C. Windsor, *Adv. Phys.* **25**, 87 (1976).
- ¹⁶C. Dupas and J. P. Renard, in *Proceedings of the 14th Conference on Low Temperature Physics*, (North-Holland, Amsterdam, 1975), Vol. 5, p. 463.
- ¹⁷A. R. McGurn, P. A. Montano, and D. J. Scalapino, *Solid State Commun.* **15**, 1463 (1974).
- ¹⁸P.-A. Lindgard and A. Kowalska, *J. Phys. C* **9**, 2081 (1976).
- ¹⁹D. Beeman and P. Pincus, *Phys. Rev.* **166**, 359 (1968).
- ²⁰In our preliminary analysis [T. Goto and Y. Yamaguchi, *J. Magn. Magn. Mater.* **31-34**, 1211 (1983)], we have compared the experimental curves with the calculated curves for the first-order process by adjusting the coupling constant properly.
- ²¹D. L. Huber, *Phys. Lett.* **71A**, 353 (1979).
- ²²See A. Abragam, *The Principles of Nuclear Magnetism* (Oxford University Press, New York, 1960), Chap. VIII.
- ²³H. J. Mikeska, *Phys. Rev. B* **26**, 5213 (1982).
- ²⁴F. Borsa, *Phys. Lett.* **80A**, 309 (1980). This paper came to the author's notice just after Ref. 8 was submitted to *J. Phys. Soc. Jpn.*